

RESEARCH ARTICLE

Wind plant power optimization through yaw control using a parametric model for wake effects—a CFD simulation study

P. M. O. Gebraad¹, F. W. Teeuwisse¹, J. W. van Wingerden¹, P. A. Fleming², S. D. Ruben³, J. R. Marden³ and L. Y. Pao³

¹ Delft Center for Systems and Control, Delft University of Technology, Delft, The Netherlands

² National Renewable Energy Laboratory, Golden, Colorado, USA

³ University of Colorado, Boulder, Colorado, USA

ABSTRACT

This article presents a wind plant control strategy that optimizes the yaw settings of wind turbines for improved energy production of the whole wind plant by taking into account wake effects. The optimization controller is based on a novel internal parametric model for wake effects called the FLOW Redirection and Induction in Steady-state (FLORIS) model. The FLORIS model predicts the steady-state wake locations and the effective flow velocities at each turbine, and the resulting turbine electrical energy production levels, as a function of the axial induction and the yaw angle of the different rotors. The FLORIS model has a limited number of parameters that are estimated based on turbine electrical power production data. In high-fidelity computational fluid dynamics simulations of a small wind plant, we demonstrate that the optimization control based on the FLORIS model increases the energy production of the wind plant, with a reduction of loads on the turbines as an additional effect. Copyright © 2014 John Wiley & Sons, Ltd.

KEYWORDS

wind plant control; wind turbine yaw control; wind turbine wakes; optimization

Correspondence

J. W. van Wingerden, Mekelweg 2, 2628CD Delft, The Netherlands.

E-mail: J.W.vanWingerden@TUDelft.nl

Received 21 February 2014; Revised 6 October 2014; Accepted 28 October 2014

1. INTRODUCTION

Each wind turbine in a cluster of wind turbines (a wind power plant) can influence the performance of other turbines through the wake that forms downstream of its rotor. The wake is a flow structure that is characterized by a reduced wind speed because the turbine rotor extracts kinetic energy from the incoming flow and an increased turbulence because the turbine obstructs the flow. If another turbine is standing in the path of a wake at a location where the flow has not yet fully recovered to free stream conditions, the reduced wind speed results in a lower electrical energy production of that turbine. In addition, the increased turbulence and shear in the wake may induce an increase in dynamic loads on the downstream turbine. These wake interaction effects have been studied extensively; see the studies of Vermeer *et al.*, Crespo *et al.* and Sanderse for reviews of the literature.^{1–3} The topology and amount of the wake interaction depend on time-varying atmospheric conditions (e.g., wind direction, wind speed, turbulence, and atmospheric stability) and on the operating point of each turbine that can be adjusted by changing their control settings (generator torque, pitch angles of the blades,⁴ or yaw angle).^{5–7}

In current industrial practice, wind turbines in wind plants are still controlled to maximize their own individual performance, ignoring the effect that the turbines have on other turbines through their wakes.⁸ Recently, the wake interaction effects have become a more significant field of study in the research on wind turbine control algorithms because wind plants have grown in size, and more knowledge has become available on the loss of efficiency because of the wake interaction effect. The study of Barthelmie *et al.*,⁹ for example, reports an average energy production loss of 12% in an offshore wind plant caused by the wake effects (this percentage is averaged over the wind directions).

Previous work on wind plant control has mainly focused on reducing wake interaction by adjusting the axial induction of turbines to improve the overall wind plant performance, which can be achieved by adjusting pitch and torque. This concept was first proposed in the late 1980s by Steinbuch *et al.*¹⁰ Static model-based optimization strategies, based on simplified parametric wake models, are tested by Johnson and Thomas⁸ and Bitar and Seiler¹¹ (based on the Jensen wake model)^{12,13} and by Gonzalez *et al.*¹⁴ (based on the Frandsen wake model).¹⁵ In the work of Schepers and van der Pijl,¹⁶ a similar static optimization is performed based on a computational fluid dynamics (CFD) model. Axial-induction-based wind plant control strategies that adjust the control settings to changing inflow conditions were developed by Marden *et al.* and Gebraad and van Wingerden (model-free data-driven approaches),^{17,18} Heer *et al.* (a model-based control approach using the Jensen model),¹⁹ and Soleimanzadeh *et al.* (model-based control approaches using simplified CFD models).^{20–22}

The goal of the work presented here is to optimize the yaw angles of the wind turbines for increased total electrical power production of the wind plant. By changing the yaw angle of a turbine, the flow direction of the wake, as well as the axial induction of the rotor, is changed. By controlling the deflection of the wake through yawing, the wake can be directed away from downstream turbines. This approach was shown to have great potential in CFD simulations in the studies of Jiménez *et al.* and Fleming *et al.*^{7,23,24} The concept was also tested in wind tunnel experiments with scaled turbines⁵ and on a small wind plant.⁶ These tests confirmed that the wake can be redirected using yaw, but since only a limited amount of data could be gathered, no quantitative analysis could be made. An interesting work in this context is that of Kragh and Hansen²⁵ in which it is shown that misaligning the rotor yaw of a turbine with the wind direction can also be used to reduce the loads on the misaligned turbine. The response of the complete wind plant system with respect to control setting changes is slow because of large delays associated with the flow in the wake traveling from one turbine to the next.^{26,27} This is a disadvantage for model-free global optimization approaches such as the one proposed by Marden *et al.*¹⁷ The long time it would take a global optimization to iteratively test control settings on the real system and converge is problematic if the controller has to adapt to time-varying conditions such as wind direction and inflow velocity. In the study of Gebraad and van Wingerden,¹⁸ the problem of having large delays in the system is addressed, and an alternative gradient-based ‘localized’ approach for model-free optimization is proposed to improve the time efficiency of the wind plant control. This localized optimization algorithm only takes into account the effect of control setting changes on the nearest downstream neighboring wind turbines. This approach was used by Gebraad and van Wingerden for pitch-based and torque-based wind plant control,¹⁸ but it is less suited for yaw control if the goal is to not only deflect the wake away from the nearest downstream turbine but also to avoid the wake hitting turbines farther downstream. Therefore, in this work, we propose a model-based control scheme, in which an optimization algorithm can test a large number of possible control settings on the model, in order to iteratively find the optimal settings based on the model predictions before applying them to the real system.

The supervisory wind plant control scheme proposed in this paper increases the total electrical energy production of the wind plant by model-based optimization of the yaw control settings. Figure 1 gives an overview of the proposed control scheme. An important part of the work presented in this paper is the development of the ‘internal model’ for the wind plant controller. The internal model predicts the wake effects in the wind plant. A preliminary version of this work appeared in the study of Gebraad *et al.*²⁸ High-fidelity CFD-based models that are based on a coupling of detailed turbine dynamics models with accurate wind flow models, such as the ones presented by Yang and Sotiropoulos, Larsen *et al.*, Churchfield *et al.* and Schepers and van der Pijl,^{29–32} have an important role in wind plant controls development, as they allow the algorithms to be tested in a controlled environment. Because of their computational complexity, accurate

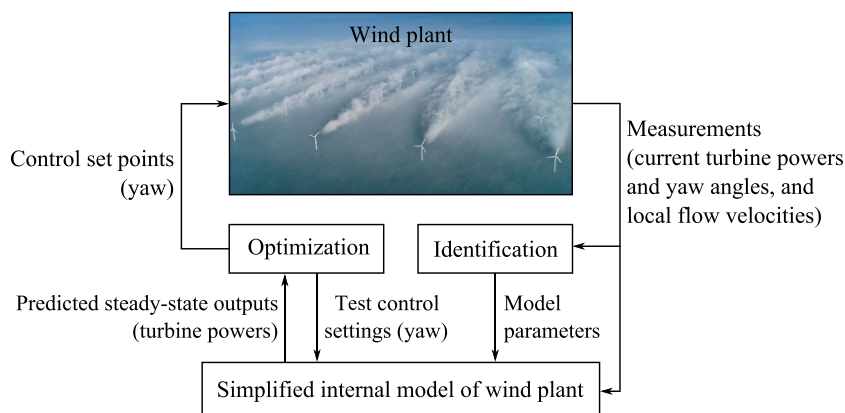


Figure 1. Overview of the data-driven model-based wind plant control optimization approach (wind plant photo courtesy: Vattenfall, C. Steiness).

CFD-based models are less suited for use as internal models for real-time controllers. The simplified parametric Jensen and Frandsen models that were used in axial-induction-based wind plant control strategies mentioned earlier^{8,11,14,19} do not include the ability to predict the effect of yaw control on wake redirection. Therefore, we have developed a novel control-oriented model that is able to predict the steady-state effects of yaw control on the wakes as well as the resulting effects on the turbine electrical power productions. The model has parameters that can be identified by fitting the predictions of the model to turbine power measurements, an approach referred to as ‘gray-box’ system identification. In addition, the model uses measurements from the wind plant to estimate relevant properties of the inflow into the wind plant. The combination of the model identification and the model-based optimization steps in the control scheme is illustrated in the overview in Figure 1. The fact that we use measurements to identify the model parameters and the inflow conditions is the reason why we refer to the control scheme as ‘data-driven’. Furthermore, the model has a relatively simple structure that allows for quick computation, meaning that it is suited for real-time control based on model-based optimization of the control settings.

Because we do not have access to a real-world wind plant on which to perform yaw control experiments, in this work, we use a high-fidelity CFD wind plant model to generate the data needed to develop the simplified parametric model and identify the model parameters. Next, we implement the model in a wind plant control scheme that performs model-based optimization of the yaw settings of each turbine using a game-theoretic (GT) approach. Finally, we test this model-based optimization control strategy in the high-fidelity wind plant simulation in which the effects on power production and loads are calculated. In this way, the high-fidelity simulation is used to provide a proof of concept for the data-driven optimization control scheme based on the simplified parametric model. Previous work on yaw optimization for wind plants³³ did not include validation of the optimized settings using high-fidelity numerical simulations.

The remainder of this paper is organized as follows. In Section 2, we describe the simulation experiments performed in the high-fidelity CFD simulator to obtain identification data for the parametric model. The simplified parametric model, called FLOw Redirection and Induction in Steady-state (FLORIS), is presented in Section 3. In Section 4, we explain the GT approach to calculate optimal yaw control settings based on the simplified model. In Section 5, we present simulation studies to validate the data-driven model-based optimization approach in the high-fidelity CFD wind plant simulation. Finally, we discuss our conclusions in Section 6.

2. CHARACTERIZING WAKE EFFECTS THROUGH SIMULATIONS IN SOWFA, A HIGH-FIDELITY CFD WIND PLANT SIMULATOR

In this section, we describe the simulations we performed in a CFD simulator to obtain identification data for the parametric model. We use the Simulator for Onshore/Offshore Wind Farm Applications (SOWFA), which is a large-eddy simulation (LES) of the three-dimensional wind flow around one or more turbine rotors in the atmospheric boundary layer. The rotating rotor blades are modeled through an actuator line approach.³ The actuator lines are coupled with the Fatigue, Aerodynamics, Structures and Turbulence (FAST) turbine aeroelastics simulator tool³⁴ that calculates the loads, power and rotor speed of each turbine, in addition to the forces that each turbine blade exerts on the flow. Each turbine in the simulation can be controlled using an individual control algorithm implemented in FAST and also through a supervisory or distributed plant-wide controller. More details on the CFD calculations in SOWFA can be found in the study of Churchfield *et al.*,³¹ and Fleming *et al.*^{35,36} give more explanation on controls implementation in SOWFA. In addition, Churchfield *et al.*³⁷ present a validation of SOWFA with time-averaged turbine powers measured at the Lillgrund wind plant in Öresund, Sweden.

SOWFA simulation results were presented by Fleming *et al.*^{23,24} that show the following:

- The effectiveness of the yaw techniques in redirecting the wake.
- The effect of yaw wake redirection techniques on the electrical energy production and loads of downstream turbines that are standing in the wake of the yawing turbine.
- The effect on electrical energy production and loads on a turbine of repositioning that turbine such that the overlap with a wake of an upstream turbine is reduced.

More in particular, Fleming *et al.*²⁴ present the results of SOWFA simulations of a setup of two National Renewable Energy Laboratory (NREL) 5-megawatt (MW) baseline turbines.³⁸ These turbines have a rotor diameter $D = 126.4$ m. In this setup, the turbines are aligned in the wind direction with a downwind spacing of 7 rotor diameters ($7D$). The turbines are placed in a domain that is 3 km (horizontal length) by 3 km (horizontal width) by 1 km (height). The turbulent inflow into the domain has a mean hub-height free-stream wind speed U_∞ of 8 m s^{-1} and a turbulence intensity of 6%. This turbulent inflow is generated by a precursor simulation of the neutral boundary layer in the same domain, with an aerodynamic surface roughness that has a low value of 0.001 m, which is typical for offshore conditions.

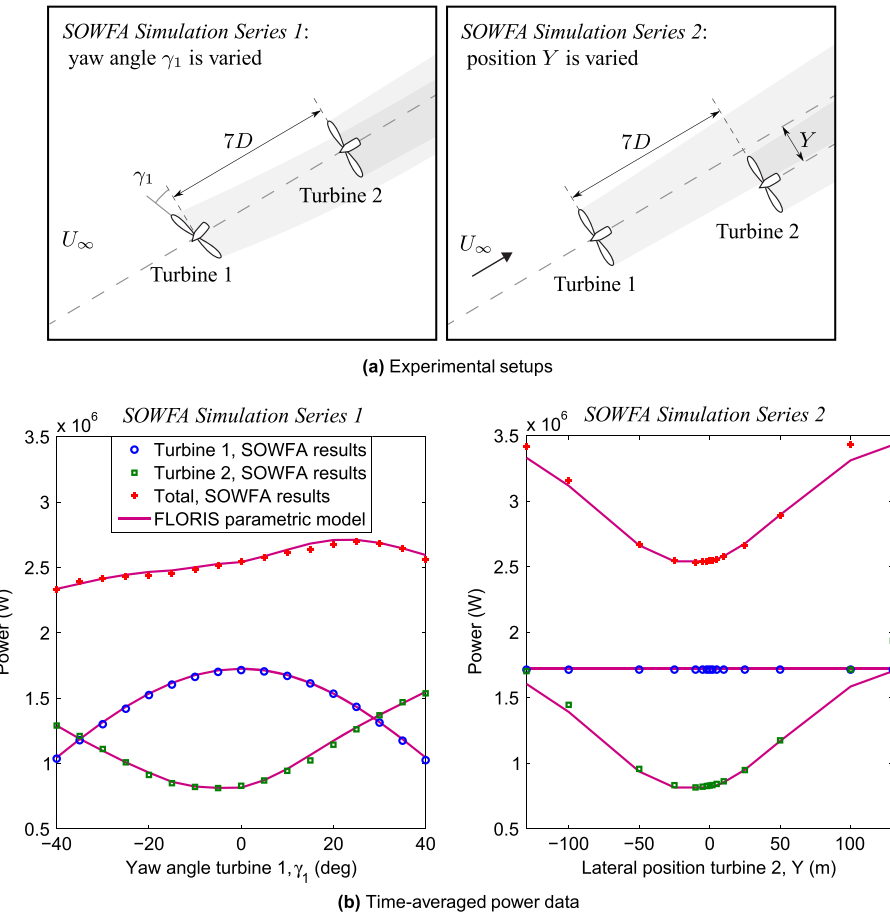


Figure 2. Setup and results for the *SOWFA Simulation Series 1* and *2* as described in Section 2. The power data were used to find the parameters of the parametric model (Section 3). (a) Experimental setups. (b) Time-averaged power data.

In this paper, we used the data from the following two series of simulations performed by Fleming *et al.*²⁴ (Figure 2(a)):

- In *SOWFA Simulation Series 1*, the upstream turbine (turbine 1) is yawed to redirect its wake away from the downwind turbine (turbine 2), resulting in an electrical power production decrease on turbine 1 caused by a loss of rotor efficiency and an electrical power production increase on turbine 2 caused by an increase of the velocity of the inflow into turbine 2.
- In *SOWFA Simulation Series 2*, turbine 2 is moved in the crosswind direction to reduce the overlap of its rotor with the wake of turbine 1, also causing an increase in the electrical power production of turbine 2.

For each yaw setting and position, a 600-s simulation was run. The wakes were allowed to develop during the first 200 s of the simulation and then 400 s of simulated data were collected. By averaging the power signals of the turbines over these 400 s, the results presented in Figure 2(b) were generated. In each case, the turbines use the baseline pitch and torque controllers defined by Jonkman *et al.*³⁸ For the simulated flow conditions, both the upstream and the downstream turbine operate in a below-rated operating region (region 2) and thus use constant pitch, variable torque control to maximize power production.^{38,39} For most cases, the downwind turbine produces less electrical energy than the upwind one because it is subjected to the low-speed wake of the upwind turbine. Figure 2(b) also includes the predictions of the simplified parametric model (FLORIS) that is presented in Section 3.

SOWFA high-fidelity CFD simulations are typically run for a few days on a cluster with a few hundred processors.^{23,24} Because of the complexity and computational costs of the SOWFA model, it is not suitable as an internal model for a wind plant controller. The data generated by SOWFA, however, can be used to develop simplified models that can be directly used by the controller. In Section 3, we describe how the power data from *SOWFA Simulation Series 1* and *2* are used to develop and identify parameters of such a simplified control-oriented model (FLORIS). In Section 5, we use SOWFA to evaluate the control techniques based on the simplified internal model in high-fidelity simulations.

3. FLORIS, A DATA-DRIVEN PARAMETRIC WIND PLANT MODEL

In this section, we explain the structure of a parametric model predicting the steady-state effects of yaw misalignment of different turbines on the electrical energy productions of wind turbines in a wind plant. It captures the effects of the yaw control on both the redirection of the wake behind the turbine and on the velocity in the wake. This is important for predicting the electrical energy productions on downstream turbines, as is also pointed out by Choi and Shan.²⁷ Since it includes both effects, for the remainder of the paper, we refer to the model as the FLORIS model.

The FLORIS model is a combination of the Jensen model^{12,13} and a model for wake deflection through yaw first presented by Jiménez *et al.*⁷ Further, augmentations were made to the Jensen model in order to better model situations with partial wake overlap and to the wake deflection model in order to include wake position offsets caused by rotor rotational effects. These augmentations also allow better fits of the model with the power measurements obtained in *SOWFA Simulation Series 1* and *2*.

Figure 3 gives an overview of the different parts of the model and of how it interacts with the yaw optimization algorithm of the wind plant controller. It also shows that *measured* power and yaw setting of turbines, as well as wind direction measurements at each turbine, are fed into the model. The measurements are used to estimate certain atmospheric conditions, being the current direction and free-stream velocity of the inflow into the wind plant. These yaw measurements should be distinguished from the preliminary test *yaw settings* that the optimization algorithm feeds into the model, and the corresponding *predicted turbine power outputs* that the model generates on the basis of those test yaw settings and the estimated inflow properties, and feeds back to the optimization algorithm.

In this section, we present the different parts of the FLORIS model. First, in Section 3.1, we explain how the electrical power production levels of the turbines are calculated (the turbine power model in Figure 3). To calculate these power levels, estimates of the effective inflow speeds are used. These inflow speed estimates follow from the wake model. In the wake model, we use a specific downwind/crosswind coordinate frame. Figure 3 shows that the turbine coordinates are transformed to these coordinates using measured wind directions at the turbines. This step is further explained in Section 3.2. Submodels for different wake properties are the wake decay, deflection and expansion models, which are also shown in Figure 3. These submodels are explained in Sections 3.3–3.5. Finally, Figure 3 shows the wake combination submodel, which defines how the wake effects of the different turbines are combined to find the effective inflow speeds

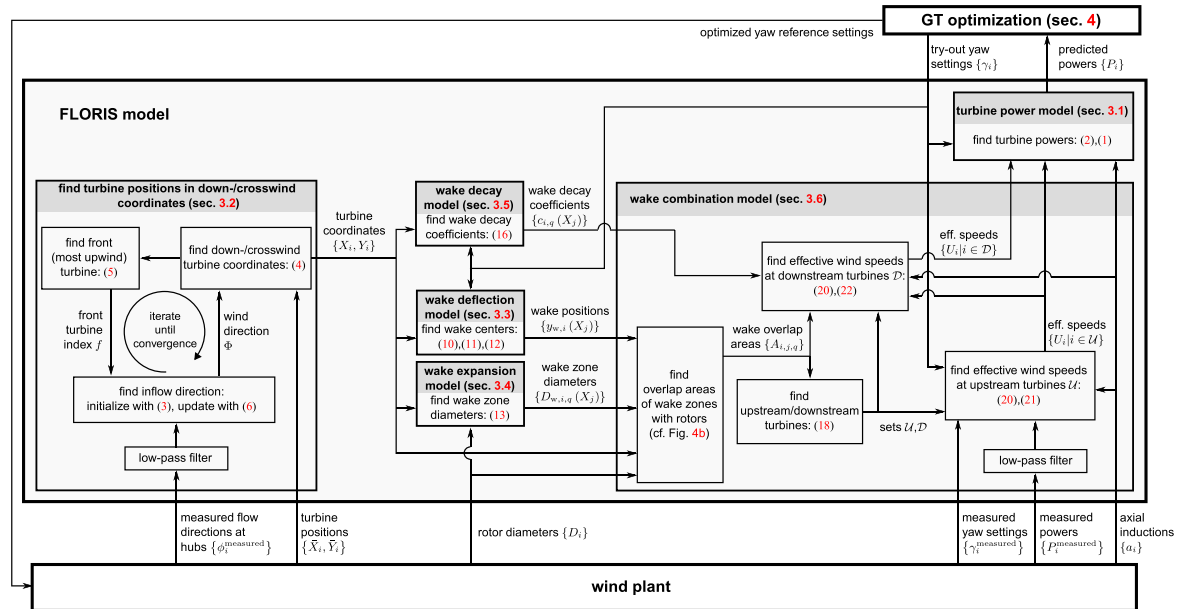


Figure 3. Overview of the FLORIS data-driven parametric model as it is implemented in the wind plant controller. Figure 1 shows the same basic control scheme, but in this figure, the different submodels of the FLORIS simplified wind plant model are shown, and the identification block is omitted. The FLORIS model uses some measurements from the wind plant (shown below the model scheme) to estimate inflow properties (speed and direction). The GT optimization algorithm (top right) uses the FLORIS model to test yaw settings for these particular inflow conditions and finally sends optimized yaw settings as reference signals to the wind plant. In the scheme shown here, the shorthand notation $\{\theta_i\}$ is used for the set $\{\theta_j | i \in \mathcal{F}\}$, where θ_j is a certain property of a turbine i in the wind plant.

at each turbine. We explain this submodel in Section 3.6. In explaining the model, we introduce different coefficients that serve as model parameters that are to be tuned to measurements from a wind plant. In this work, we use the power measurements from SOWFA to find the FLORIS model parameters, as discussed in Section 3.7.

3.1. Turbine power

Let $\mathcal{F} = \{1, 2, \dots, N\}$ denote a set of indices that number the wind turbines in a wind plant, with N denoting the total number of turbines in the plant. The steady-state electrical power of a turbine $i \in \mathcal{F}$, denoted as P_i , is calculated as follows:⁴⁰

$$P_i = \frac{1}{2} \rho A_i C_P(a_i, \gamma_i) U_i^3 \quad \forall i \in \mathcal{F} \quad (1)$$

where ρ is the air density, A_i is the rotor swept area, C_P is the power coefficient of the turbine, and U_i is the effective wind speed at the turbine. In nonyawed idealized conditions, the power coefficient is related to the axial induction factor of each turbine, defined as $a_i = 1 - U_{i,D}/U_i$, with $U_{i,D}$ being the wind speed at the rotor, and U_i the free-stream wind speed in front of turbine i , as $C_P(a_i) = 4a_i[1 - a_i]^2$.⁴⁰ In the model presented here, we apply a correction on this relationship to account for the effect of the yaw misalignment angle γ_i on the rotor power coefficient, following the example of the experimental studies by Medici.⁴¹ In addition, we use a constant scaling of the C_P value, η , to account for other losses. This results in

$$C_P(a_i, \gamma_i) = 4a_i[1 - a_i]^2 \eta \cos(\gamma_i)^{pp} \quad (2)$$

To match the maximum $C_P = 0.482$ and 94.4% generator efficiency reported by Jonkman *et al.*³⁸ for the NREL 5-MW turbine that is used in *SOWFA Simulation Series 1* and 2, we use a loss factor $\eta = 0.768$. In the study of Medici,⁴¹ a parameter value $pp = 2$ was found to fit data from wind tunnel tests with yawing turbines, but the parameter settings listed in Table I are found to fit the yaw-power relationship of the upstream turbine (turbine 1) in *SOWFA Simulation Series 1* (Figure 2(b)). To find these parameters, we assume an idealized axial induction of $a_i = 1/3$ for below-rated conditions. The model can be extended to above-rated operation by make corrections on a_i as a function of inflow speed U_i (based on a maximum rated power), or by making a_i a function of pitch and tip-speed ratio, using knowlegde of the C_P -curve.

In the remainder of this section, we describe how the effective inflow speeds U_i at each turbine are estimated by the model by predicting the steady-state wake characteristics as a function of the yaw angles.

3.2. Inflow direction and the downwind–crosswind coordinate frame

To describe the spatial properties of the wakes behind the turbines, we adopt a Cartesian coordinate framework (x, y) in which the x -axis is pointing downwind along an estimated mean inflow direction in the wind plant, and the y -axis is pointing orthogonal to the x -axis in the horizontal direction (i.e., along the crosswind direction, as illustrated in Figure 4). The z -axis then represents the altitude. In this work, we assume that each turbine has the same hub-height, and the turbine locations in this downwind–crosswind coordinate frame are denoted as $(X_i, Y_i) \forall i \in \mathcal{F}$.

The mean inflow direction, denoted by Φ , can be estimated in several ways. In the model, as used in the CFD simulation examples in Section 5, it is found using wind direction measurements at the most upwind turbine. To determine which is the front turbine, we need some initial guess of the free-stream wind direction, so we use the iterative procedure described in the numbered list that follows. The steps of this procedure are also illustrated in the left-most block in the FLORIS model scheme in Figure 3. The steps are as follows:

1. We average the flow direction measurements at the hub of each turbine $i \in \mathcal{F}$, denoted as ϕ_i^{measured} , to provide a first estimate of the inflow direction. In the CFD simulation examples, the wind direction at the turbine hubs is estimated by sampling the horizontal velocity components (\bar{u}_i, \bar{v}_i) at the hub location of each turbine $i \in \mathcal{F}$ from the flow field

Table I. Parametric model parameters.

Turbine power	Wake						
	Deflection		Expansion		Velocity		
η	0.768	k_d	0.15	k_e	0.065	$M_{U,1}$	0.5
p_P	1.88	a_d	-4.5	$m_{e,1}$	-0.5	$M_{U,2}$	1
		b_d	-0.01	$m_{e,2}$	0.22	$M_{U,3}$	5.5
				$m_{e,3}$	1	a_U	5
						b_U	1.66

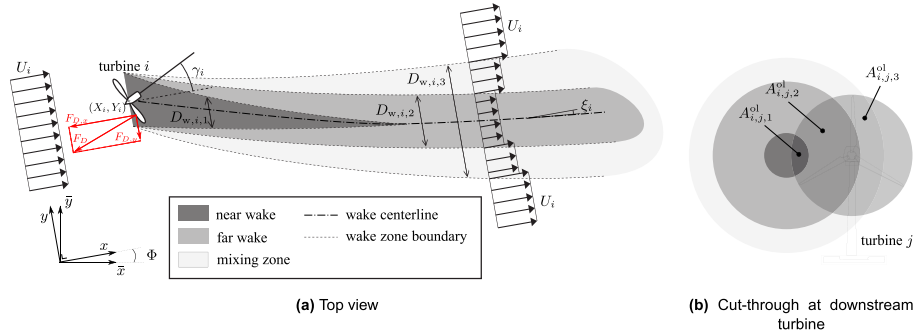


Figure 4. The three different wake zones of the parametric model. The free-stream wind vectors are indicated as arrows with length U_i (the free-stream velocity). Inside the wake zones, the wind vectors have a reduced velocity (Section 3.5). The areas overlapping with a downstream rotor j , $A_{i,j,q}^{\text{ol}}$, are used to calculate the effective wind speed at turbine j (equations (20) and (22)). (a) Top view. (b) Cut-through at downstream turbine.

calculated by the CFD simulator and by calculating the direction in the horizontal plane as $\phi_i = \tan^{-1}(\bar{v}_i/\bar{u}_i)$:

$$\Phi = \frac{1}{N} \sum_{i=1}^N \phi_i^{\text{measured}} \quad (3)$$

2. The turbine positions in downwind/crosswind coordinates are calculated according to the estimated wind direction. If $\{\bar{X}_i, \bar{Y}_i\}$ are the turbine coordinates relative to the same Cartesian coordinates (\bar{x}, \bar{y}) to which the wind direction Φ is measured (Figure 4), the downwind–crosswind turbine coordinates are

$$\begin{bmatrix} X_i \\ Y_i \end{bmatrix} = \begin{bmatrix} \cos(-\Phi) & -\sin(-\Phi) \\ \sin(-\Phi) & \cos(-\Phi) \end{bmatrix} \begin{bmatrix} \bar{X}_i \\ \bar{Y}_i \end{bmatrix} \quad (4)$$

3. It is established which turbine is the front (most upwind) turbine, and it is assumed that the mean inflow direction is equal to the wind direction measured at that turbine (i.e., we assume a uniform direction of the free-stream inflow to the wind plant):

$$f = \arg \min_{i \in \mathcal{F}} X_i \quad (5)$$

$$\Phi = \phi_f^{\text{measured}} \quad (6)$$

4. We repeat steps 2 and 3 until convergence (i.e., no change in estimated wind direction Φ).

The wind direction estimation iterative procedure will generally converge to a wind direction measured at a certain turbine within two or three iterations in our simulation examples. Note that in our implementation of the model as illustrated in Figure 3, the wind direction measurements at the hub of the turbines, defined relative to the mesh coordinates, are low-pass filtered to filter out small-scale turbulence effects.

3.3. Wake deflection

Yawing a turbine rotor causes the thrust force that the rotor exerts on the flow, F_D , to rotate in such a way that a crosswind component is induced,⁷ which causes the wind flow to deflect in the direction opposite to the yaw rotation (Figure 4(a)). Because the wake deflection is induced by the thrust force, the amount of deflection is a function of the thrust coefficient of the turbine $C_T = 2F_D / (\rho A_i U_i^2)$. When the yaw is not misaligned with respect to the wind direction (i.e., $\gamma_i = 0$), the thrust coefficient is related to the axial induction factor a_i of the rotor of a turbine i as follows:⁴⁰

$$C_T(a_i) = 4a_i[1 - a_i] \quad (7)$$

The following heuristic relationship between the yaw angle of a turbine i, γ_i , the thrust factor C_T of the turbine in nonyawed conditions and the angle of the centerline of its wake ξ_i at a downstream location $x > X_i$ was derived in the study of Jiménez *et al.*:⁷

$$\xi_i(x) \approx \frac{\xi_{\text{init}}(a_i, \gamma_i)^2}{\left[1 + 2k_d \frac{x-X_i}{D_i}\right]} \quad \text{with } \xi_{\text{init}}(a_i, \gamma_i) = \frac{1}{2} \cos^2(\gamma_i) \sin(\gamma_i) C_T(a_i) \quad (8)$$

where D_i is the rotor diameter of turbine i , k_d is a model parameter that defines the sensitivity of the wake deflection to yaw and where ξ_{init} is the initial angle of the wake at the rotor. Relation (8) is elegant in the sense that it only has one unknown parameter, k_d , to be tuned. This k_d parameter defines the recovery of the wake flow direction toward the main inflow direction Φ . By integrating the tangent of the wake centerline angle over x , the yaw-induced lateral offset of the wake center with respect to the hub of a turbine i , denoted as $\delta y_{w,yaw,i}$, can be found:

$$\delta y_{w,yaw,i}(x) = \int_0^{x-X_i} \tan(\xi_i(x)) dx \quad (9)$$

This integral can be approximated by integrating the second-order Taylor series approximation of $\xi(x)$, yielding

$$\delta y_{w,yaw,i}(x) \approx \frac{\xi_{\text{init}}(a_i, \gamma_i) \left[15 \left[\frac{2k_d[x-X_i]}{D_i} + 1 \right]^4 + \xi_{\text{init}}(a_i, \gamma_i)^2 \right]}{\frac{30k_d}{D_i} \left[\frac{2k_d[x-X_i]}{D_i} + 1 \right]^5} - \frac{\xi_{\text{init}}(a_i, \gamma_i) D_i [15 + \xi_{\text{init}}(a_i, \gamma_i)^2]}{30k_d} \quad (10)$$

In addition, in the simulations described by Fleming *et al.*,²³ it was shown that a small lateral wake deflection occurs when the turbine is not yawed (i.e., $\gamma_i = 0$). This deflection can be explained by vertical shear in the boundary layer and wake rotation. In reaction to the rotor rotating clockwise, the wake will rotate counterclockwise. As a result, the low-speed flow in the lower part of the boundary layer will be rotated up and to the right, and high-speed flow in the upper part of the boundary layer will be rotated down and to the left. Consequently, the velocity deficit at the right part of the wake (looking downstream) increases, so the wake deflects to the right. Because in *SOWFA Simulation Series 1* and *2*, the wake behavior was tested for a single mean wind velocity with a limited velocity variation caused by turbulence, the exact dependence of the wake deflection on the rotor speed could not be derived from the power data obtained. Therefore, this rotation-induced wake lateral offset is parameterized through a simple linear function of the downstream distance from the rotor:

$$\delta y_{w,rotation,i}(x) = a_d + b_d [x - X_i] \quad (11)$$

Combining the rotation-induced and yaw-induced components, the position of the wake center of a turbine i at a downstream location $x > X_i$ is given by

$$y_{w,i}(x) = Y_i + \delta y_{w,rotation,i}(x) + \delta y_{w,yaw,i}(x) \quad (12)$$

3.4. Wake expansion

The Jensen model^{12,13} assumes a wake that is expanding proportionally to the axial downstream distance from the rotor and a wind velocity in the wake that is uniform in the lateral direction. In reality, the velocity will recover to the free-stream velocity faster toward the edges of the wake.³ Therefore, we expand the Jensen model to better model partial wake situations by dividing the wake in three zones that also expand proportionally with the distance from the rotor but each with their own expansion factor (Figure 4(a)). The diameters of the wake zones behind a turbine i are given by

$$D_{w,i,q}(x) = \max(D_i + 2k_e m_{e,q}[x - X_i], 0) \quad (13)$$

for $x > X_i$, and index $q = 1, 2, 3$ numbering the different zones, D_i being the rotor diameter of turbine i and with parameters $m_{e,q}, k_e$ being coefficients that define the expansion of the zones. The different wake zones are the ‘near wake’ ($q = 1$), ‘far wake’ ($q = 2$) and ‘mixing zone’ ($q = 3$), in accordance with the terms that are commonly used in literature to describe wake characteristics.^{1–3} The scaling parameter for the expansion of the near wake, $m_{e,1}$, is typically set to a negative value, which prescribes that the cross-section of the near wake zone is decreasing to zero with the distance to the rotor. The extension to different wake zones allows us to better match the data from *SOWFA Simulation Series 1* and *2* (Section 3.7).

3.5. Wind velocity in a single wake

By definition, the axial induction is the relative amount of velocity drop at the rotor with respect to the inflow velocity. From actuator disk theory, it follows that the relative rotor-induced drop of the velocity behind the rotor is two times the axial induction factor.⁴⁰ In the wake behind the rotor, the velocity will gradually recover to the free-stream velocity by turbulence-induced mixing. The Jensen model assumes that the time-averaged velocity deficit in the far wake decays quadratically with the expansion of the wake. In the study of Annoni *et al.*,⁴² it is shown that the parameters of the Jensen model can be tuned to obtain a good fit of the time-averaged velocity profile in the far wake as predicted by the SOWFA model for nonyawed conditions. An extension made in the FLORIS model, done to better fit the power data from *SOWFA Simulation Series 1* and *2*, is that the wake is divided into three zones, as described in the previous section, and that the velocity deficit decays quadratically with the distance from the rotor rather than being directly related to the wake expansion. The velocity profile behind a turbine i , then, is modeled as

$$U_{w,i}(x, y) = U_i [1 - 2a_i c_i(x, y)] \quad (14)$$

for $x > X_i$, with U_i again denoting the free-stream speed in front of the turbine. The wake decay coefficient, $c_i(x, y)$, is a piecewise constant function of the lateral offset of the location y with respect to the wake center of turbine i , defined as

$$c_i(x, y) = \begin{cases} c_{i,1} & \text{if } |r| \leq D_{w,i,1}(x)/2 \\ c_{i,2} & \text{if } D_{w,i,1}(x)/2 \leq |r| \leq D_{w,i,2}(x)/2 \\ c_{i,3} & \text{if } D_{w,i,2}(x)/2 \leq |r| \leq D_{w,i,3}(x)/2 \\ 0 & \text{if } |r| > D_{w,i,3}(x)/2 \end{cases} \quad (15)$$

with $r = y - y_{w,i}(x)$

with the local wake decay coefficient for each zone given by

$$c_{i,q}(x) = \left[\frac{D_i}{D_i + 2k_e m_{U,q}(\gamma_i)[x - X_i]} \right]^2 \quad (16)$$

The coefficients $m_{U,q}$ are parameters defining how quickly the different wake zones decay. Following a similar approach to that described in Section 3.1, the wake decay rates are adjusted for the rotor yaw angle to fit the data from *SOWFA Simulation Series 1* and *2* by empirically deriving the following relationship between the coefficient $m_{U,q}$ and the yaw angle γ_i :

$$m_{U,q}(\gamma_i) = \frac{M_{U,q}}{\cos(a_U + b_U \gamma_i)} \quad (17)$$

for $q = 1, 2, 3$ with model parameters $M_{U,q}, a_U, b_U$.

3.6. Combining wakes to find the turbine effective wind velocities

In the submodel described in this section, we combine the effects of the wake zones of different turbines to estimate the effective inflow velocity at each turbine. The different parts of this submodel are illustrated in the lower-right block in the FLORIS model scheme in Figure 3. The submodel described in Section 3.5 estimates the velocity deficits in the wake with respect to a certain free-stream inflow speed. Generally, we cannot assume that the free-stream inflow velocity into the wind plant is known, but by inverting the relationship in equation (1), we can estimate the effective wind speeds at the front turbines from turbine power and yaw angle measurements, denoted as P_i^{measured} and $\gamma_i^{\text{measured}}$, respectively. Next, the wind speeds at the downstream turbines are estimated by combining the effect of the wakes, weighting the wake zones by their overlap with the rotors using the root-sum-square method of Katic *et al.*¹³ This results in the following formulations.

First, the overlapping areas between turbine rotors and the different zones of the wakes are calculated from the wake center and wake diameter predictions described in Sections 3.3 and 3.4, using basic geometry. We denote the overlapping area between a wake zone q of a turbine i and a rotor of a downstream turbine j , by $A_{i,j,q}^{\text{ol}}$ (Figure 4(b)). Then, we define $\mathcal{U} \subset \mathcal{F}$ as the set of front, upstream turbines that are not influenced by other turbines through wake interaction because their rotors do not overlap with any wakes, and we define \mathcal{D} as the set of turbines that are influenced by other turbines as follows:

$$\begin{aligned} \mathcal{U} &= \left\{ j \in \mathcal{F} \mid A_{i,j,q}^{\text{ol}} = 0 \forall i \in \mathcal{F}, q \in \{1, 2, 3\} \right\} \\ \mathcal{D} &= \{ j \in \mathcal{F} \mid j \notin \mathcal{U} \} \end{aligned} \quad (18)$$

In addition, $u(j)$ denotes the index of a turbine in the set \mathcal{U} that has the largest overlap area with a turbine $j \in \mathcal{D}$ when compared with other turbines in the set \mathcal{U} :

$$u(j) = \arg \max_{i \in \mathcal{U}} \left(\sum_{q=1}^3 A_{i,j,q}^{\text{ol}} \right) \forall j \in \mathcal{D} \quad (19)$$

Figure 5 illustrates how the sets \mathcal{U} and \mathcal{D} and the mapping $j \rightarrow u(j)$ are defined in an example case. The effective inflow speed at a turbine $j \in \mathcal{D}$ is assumed to be the velocity at turbine $\rightarrow u(j)$ multiplied with a factor that represents the effects of the different wake zones, which are weighted by the overlap of these wake zones with the rotor. This results in the following relationships for estimating the effective wind speeds U_j at each turbine $j \in \mathcal{F}$:

$$U_j = \begin{cases} f_1(j) & \forall j \in \mathcal{U} \\ f_2(j) & \forall j \in \mathcal{D} \end{cases} \quad (20)$$

with functions

$$f_1(j) = \left[\frac{2P_j^{\text{measured}}}{\rho A_j C_P (a_j, \gamma_j^{\text{measured}})} \right]^{1/3} \quad (21)$$

$$f_2(j) = U_{u(j)} \left[1 - 2 \sqrt{\sum_{i \in \mathcal{F}: X_i < X_j} \left[a_i \sum_{q=1}^3 c_{i,q}(X_j) \min \left(\frac{A_{i,j,q}^{\text{ol}}}{A_j}, 1 \right) \right]^2} \right] \quad (22)$$

3.7. Fitting the wake model parameters

By fitting to the power data from turbine 2 in *SOWFA Simulation Series 1* and 2, the parameters for wake deflection, wake expansion and wake decay were tuned ‘manually’ (see Figure 2(b) and Table I). The results were validated by comparing the resulting wake velocity profiles for a single yawed turbine with the corresponding data generated by SOWFA in the simulation experiments described by Fleming *et al.*,²³ see Figure 6 for this comparison. We can see that by dividing the wake in different zones, as described in Section 3.4, and introducing a rotation-induced wake position offset (Section 3.3), we are able to better match the wake velocity profile.

4. WIND PLANT YAW OPTIMIZATION USING A GAME-THEORETIC APPROACH

In this work, we use the GT approach of Marden *et al.*¹⁷ to perform an optimization of the yaw settings of the turbines in a wind plant with the objective of maximizing the total wind plant power production. The GT approach performs the optimization by making random perturbations to the yaw settings and holds the settings as a baseline setting if they yield an improvement of the wind plant total power so as to iteratively find the global maximum of the wind plant total power. Following the control scheme of Figure 1 (shown in more detail in Figure 3), the optimization is based on the turbine power predictions of the FLORIS model. The randomized search of the GT approach is performed using the FLORIS simplified model, and once the optimized settings are found, they are applied on the wind plant. In this section, we explain the optimization algorithm in more detail. A specification of the different parameters of the optimization algorithm for a particular case study follows in Section 5.2.

In Algorithm 1, the (simplified) optimization scheme of the GT approach is given as it is implemented in our simulation examples. The randomized perturbation on the yaw settings of the turbines in the wind plant model takes place in lines 9 through 15 of the algorithm. In lines 10 and 11, a randomized process determines whether the yaw setting of a specific turbine is updated; E is the probability of using a new random setting for γ_i , instead of keeping the baseline setting, denoted by $\bar{\gamma}_i$. By setting this search rate E , we can control the number of updates on turbines taking place at the same time and tune the convergence properties of the GT algorithm in this way. If the yaw setting of a turbine is indeed updated, it is randomly selected from the range $[\gamma_{\min}, \gamma_{\max}]$ (in lines 12 and 13). This range of possible yaw settings is discretized with an interval $\Delta\gamma$ in order to improve the convergence speed. Testing whether the updated yaw settings improve the total wind plant power, based on an evaluation of the FLORIS model, takes place in lines 18 through 22. If they yield an improvement, the updated yaw settings are stored as a baseline setting $\bar{\gamma}_i$ (line 20). After that evaluation, a new iteration of the GT algorithm will follow.

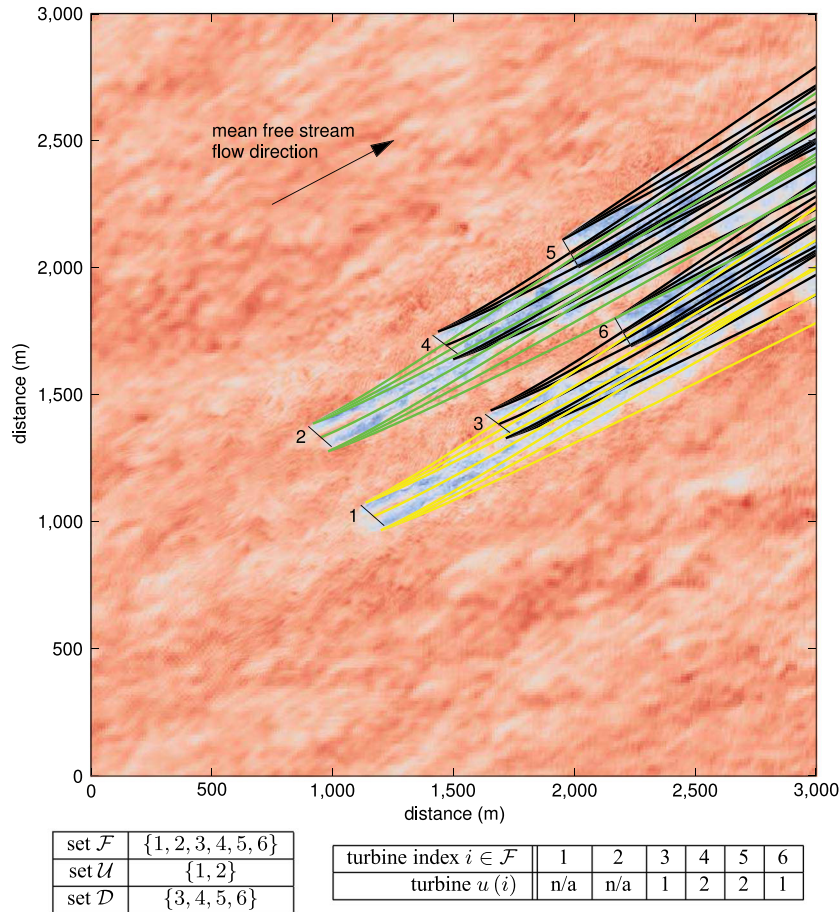


Figure 5. This picture shows the hub-height flow field of a 3×2 wind plant, with the centerline and boundaries of the wake zones as predicted by the FLORIS model shown as solid lines. The set definitions for this case, $\mathcal{F}, \mathcal{U}, \mathcal{D}$, and the mapping $i \rightarrow u(i)$ are shown in the table underneath the picture. The mapping $i \rightarrow u(i)$ follows from the fact that the rotors of turbines 3 and 6 have the largest overlap with the model-predicted wake of turbine 1 (shown in yellow), when compared with other turbines in the set \mathcal{U} , and the rotors of turbines 4 and 5 have the largest overlap with the wake of turbine 2 (shown in green).

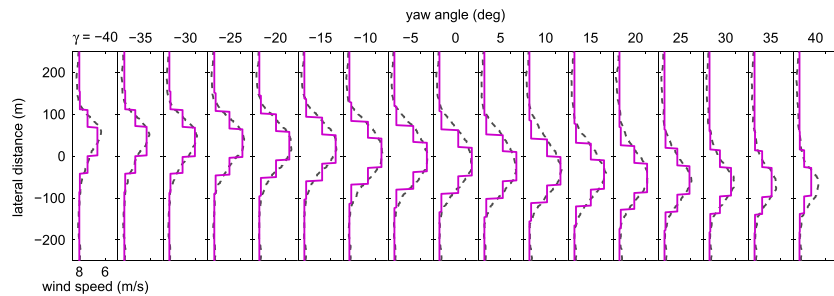


Figure 6. Time-averaged wake velocity profiles at turbine hub-height at a 7 rotor diameter distance from the rotor, for different yaw angles of the rotor γ , as calculated with SOWFA (dashed) in the simulation described by Fleming *et al.*²³ and with the FLORIS model (solid).

5. WIND PLANT YAW OPTIMIZATION SIMULATION EXAMPLES

We evaluate the online yaw optimization wind plant control strategy based on the FLORIS parametric model by using it in SOWFA simulations of a small wind plant.

Algorithm 1 The pseudocode below shows a GT approach for wind plant control, performing optimization of the yaw angles for increased electrical energy production. Index k denotes the iterations of the optimization. The variables $\bar{\gamma}_i$ and \bar{P}_i are used to store baseline values of the control variables and the corresponding turbine powers (yielding the maximum wind plant power found so far). \mathcal{U} denotes a uniform distribution, \mathbb{Z}_n denotes the set of integers $[0, 1, \dots, n]$.

```

1:  $\gamma_i \leftarrow 0 \forall i \in \mathcal{F}$ 
2:  $k \leftarrow 0$ 
3:  $n \leftarrow \frac{\gamma_{\max} - \gamma_{\min}}{\Delta\gamma}$ 
4: update  $P_i(\gamma_i) \forall i \in \mathcal{F}$  using equations (20),(1)
5:  $\bar{P} \leftarrow \sum_{i=1}^N P_i(t)$ 
6:  $\bar{\gamma}_i \leftarrow \gamma_i$ 
7: loop
8:    $k \leftarrow k + 1$ 
9:   for all  $i \in \mathcal{F}$  do
10:     $\mathcal{R}_1 \leftarrow$  random value  $\sim \mathcal{U}(0, 1)$ 
11:    if  $\mathcal{R}_1 < E$  then
12:       $\mathcal{R}_2 \leftarrow$  random value from the set  $\mathbb{Z}_n$ 
13:       $\gamma_i \leftarrow \gamma_{\min} + \mathcal{R}_2 \Delta\gamma$ 
14:    else
15:       $\gamma_i \leftarrow \bar{\gamma}_i$ 
16:    end if
17:   end for
18:   update  $P_i \forall i \in \mathcal{F}$  using equations (20),(1)
19:   if  $\sum_{i=1}^N P_i(\gamma_i) > \bar{P}$  then
20:      $\bar{\gamma}_i \leftarrow \gamma_i \forall i \in \mathcal{F}$ 
21:      $\bar{P} \leftarrow \sum_{i=1}^N P_i(t)$ 
22:   end if
23: end loop

```

5.1. Simulation setups

The simulated wind plant consists of two rows with three NREL 5-MW baseline turbines each,³⁸ with a 5 rotor diameter spacing in the downwind direction and 3 rotor diameters in the crosswind direction. We simulate a constant wind direction, and three configurations of the wind plant in which the setup is rotated 0°, 5° and 10° with respect to the wind direction. For each of these configurations, we run simulations of two cases:

- A case with the model-based control performing plant-wide optimization of the yaw settings enabled.
- A case in which the yaw settings that yield maximum power for each individual turbine are used, i.e., each rotor is aligned perpendicular to the mean wind direction. This is the conventional way in which yaw is controlled on wind turbines. Because these yaw settings result in maximization of electrical power of the turbine itself but not in production maximization on a plant level, we refer to these settings as ‘greedy’.

Figure 7 shows the turbine positions and the SOWFA-calculated flow fields for each of the cases. In this figure, we can see that yaw misalignment does lead to a redirection of the wake and an increase of flow velocity in the wake (caused by a reduction of axial induction of the rotors).

In these SOWFA simulations, we use an inflow with a 6% turbulence intensity and an 8 ms⁻¹ mean velocity, which is the same inflow condition as in *SOWFA Simulation Series 1* and 2 described in Section 2. Note that a different spacing between the turbines in the wind direction is used in *SOWFA Simulation Series 1* and 2 to obtain the parameters of the FLORIS model, namely 7 rotor diameters, and in that sense, we use the model for extrapolation. The wind plant setup is placed in a 3 km (horizontal length) by 3 km (horizontal width) by 1 km (height) mesh (Figure 7). The smallest mesh cells for the CFD calculation, which contain the turbine rotors, the axial induction zones of the rotor and the wakes between the turbines have a size of 3 m × 3 m × 3 m. Farther away from the turbines, the mesh is coarsened to 6 m × 6 m × 6 m cells and then to 12 m × 12 m × 12 m cells, resulting in a total of 32×10^6 cells. Using a time step of 0.02 s, a 1000 s simulation is performed for each of the six cases. Because of the high mesh and time resolution required, the computational cost of the CFD simulations is high: 59 h of distributed computation on 512 processors for each 1000 s simulation.

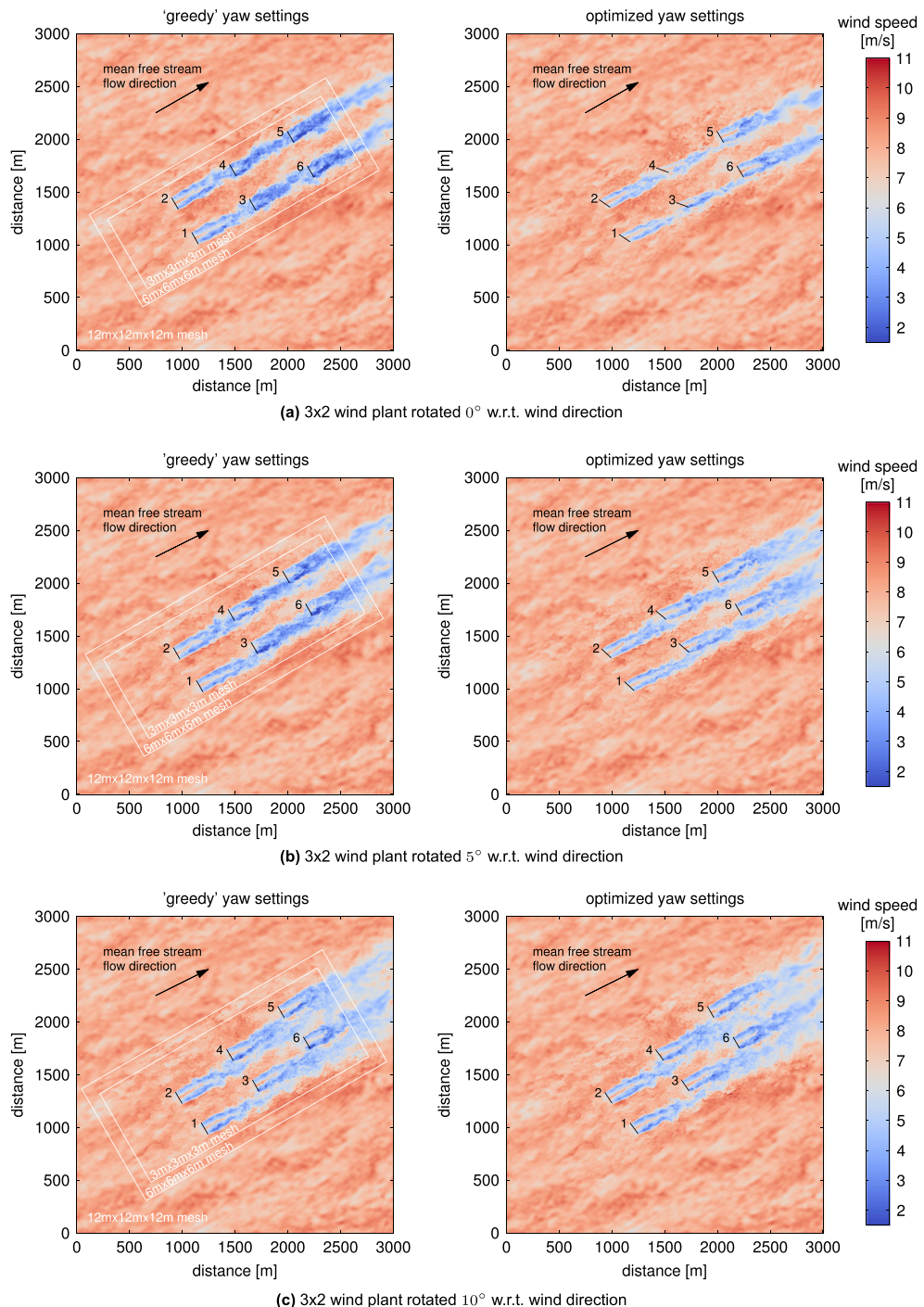


Figure 7. Hub-height wind field at 800 s simulated time as calculated by SOWFA for three different configurations of the wind plant. Black lines indicate rotor positions and yaw orientation of each turbine (the yaw angles are listed in Table III). (a) 3 × 2 wind plant rotated 0° w.r.t. wind direction; (b) 3 × 2 wind plant rotated 5° w.r.t. wind direction; (c) 3 × 2 wind plant rotated 10° w.r.t. wind direction.

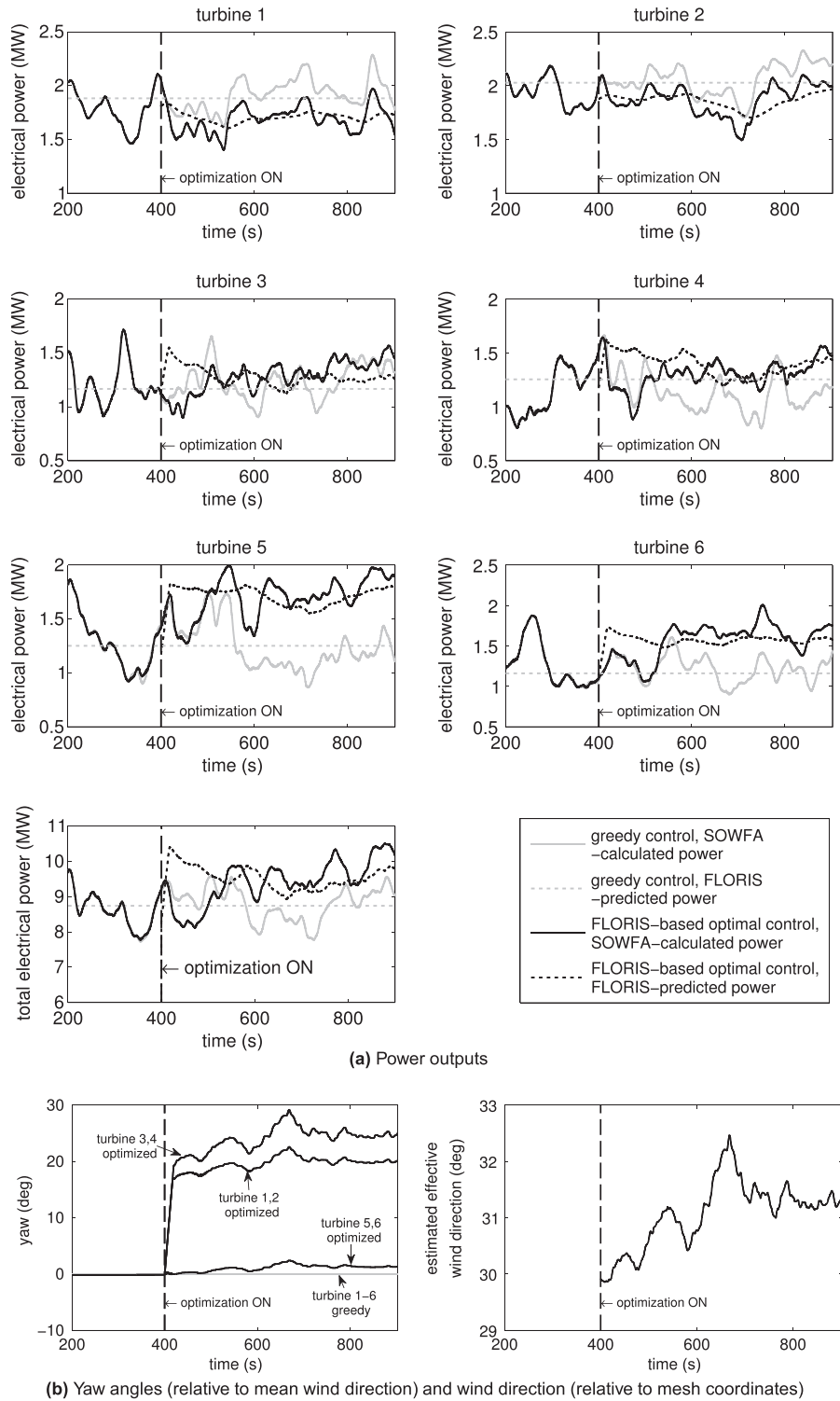


Figure 8. SOWFA simulation results and FLORIS predictions of power productions with and without FLORIS-based optimization control (a), and the yaw angles used in these simulations (b), for the 5° rotated wind plant configuration (Figure 7b). (a) Power outputs. (b) Yaw angles (relative to mean wind direction) and wind direction (relative to mesh coordinates).

5.2. Specifications of the plant-wide optimization controller used in the simulation examples

In accordance with the scheme in Figure 3, the electrical power production, yaw and local wind direction measurements as calculated by SOWFA are directly fed into the internal FLORIS model. The FLORIS model uses these signals to estimate the inflow properties (effective wind speed and direction). A first-order low-pass filter with a -3 dB cut-off frequency of 2 mHz is used on the measured power and wind direction signals to make sure that the wind plant yaw controller only responds to the slower trends in the changes of the inflow conditions. When the plant-wide controller is switched on, the yaw optimization is performed in each 0.02 s time step of the simulation. The GT algorithm parameters are set to $\gamma_{\min} = 0^\circ$, $\gamma_{\max} = 40^\circ$ (offset relative to wind direction), $\Delta\gamma = 0.05^\circ$, $E = 0.2$, and in each optimization 1000 iterations of the yaw settings are tested on the internal FLORIS model. This number of iterations is sufficient for convergence to a maximum in the predicted power production. In each iteration of the optimization it takes about 0.04 ms to evaluate the C-implementation of the FLORIS model on a single processor. The search is restricted to positive yaw angles because a previous simulation study²³ showed that for the given inflow conditions, yawing in the positive direction yields a reduction of relevant structural loads on the turbine, and negative yaw increases blade loads. After the optimization procedure, the baseline yaw setting for each turbine as calculated by the optimization algorithm is set as a reference to which the turbines respond with a maximum yaw rate of 1°s^{-1} . In the following time step, the optimization is initialized with the previous yaw reference setting.

In this case study, we used an unrealistically high update rate for the yaw reference settings when considering the maximum yaw rate of 1°s^{-1} . In practice, one would run the optimization algorithm far less frequently, and the 0.04 ms needed to run the optimization would be sufficiently short to allow for online optimization. The time between yaw reference updates on a real wind turbine may be in the order of tens of seconds to minutes (examples are discussed by Hau⁴³ and Kragh *et al.*⁴⁴). Both the conventional greedy yaw control system and the proposed plant-level optimized yaw control system respond to changes of the wind direction. The yaw reference update rate can be adjusted to make a trade-off between additional yaw actuator usage and electrical power production, where in principle, the plant-level optimized scheme does not need more actuator usage than the greedy scheme.

5.3. Detailed results of simulations with the 5-degree rotated wind plant

For the cases with the 5° rotated wind plant, relevant signals are shown in Figure 8. We compare the SOWFA simulation with the greedy settings, with a SOWFA simulation in which the plant-wide optimization controller is switched on after 400 s. Figure 8(a) compares the electrical power output calculated by SOWFA and predicted by the FLORIS model for both cases. Figure 8(b) shows the yaw angles for both cases, along with the wind direction estimated by the controller.

Figure 8(a) shows that the predictions given by FLORIS do not always closely match the SOWFA results for each turbine. This is because the FLORIS model does not include the transient effects related to the wakes taking some time to propagate through the wind plant. In addition, higher-frequency variations related to turbulence are not included in the FLORIS model. Still, the FLORIS-model predictions are accurate enough to be used by the GT optimization algorithm in the controller for the calculation of yaw settings that yield a significant increase in total power production of the wind plant, when compared with the case with the greedy settings (see lower-left plot in Figure 8(a)). In the SOWFA results, over the period of 50 – 500 s after plant-wide optimization control is switched on, 13% more electrical energy is produced on average compared with the greedy yaw case. In Figure 8(b), it can be seen that the online implementation of the GT model-based optimization responds to changes in the inflow conditions (direction and velocity), which are predicted based on the measured signals.

Table II. Total wind plant electrical power production in the SOWFA simulation results, and as predicted by the FLORIS model, for both greedy control and plant-wide optimized yaw control.

	Greedy yaw			Optimized yaw			Increase (%)
	SOWFA (MW)	FLORIS (MW)	Error (%)	SOWFA (MW)	FLORIS (MW)	Error (%)	
Wind plant rotated 0°	6.68	6.34	5.27	7.55	7.66	1.55	13.03
Wind plant rotated 5°	8.75	8.75	0.08	9.91	9.99	0.79	13.19
Wind plant rotated 10°	10.80	11.04	2.23	10.91	11.22	2.76	1.04

The data are averaged over a period of 50 – 500 s after plant-wide optimization control is switched on (and over the same period for the greedy case). Also listed are the errors of the FLORIS prediction relative to the SOWFA results and the increase obtained when using optimized yaw relative to the greedy yaw control case in the SOWFA results.

P. M. O. Gebraad, F. W. Teeuwisse et al.

Wind plant power optimization through yaw control using a parametric wake model

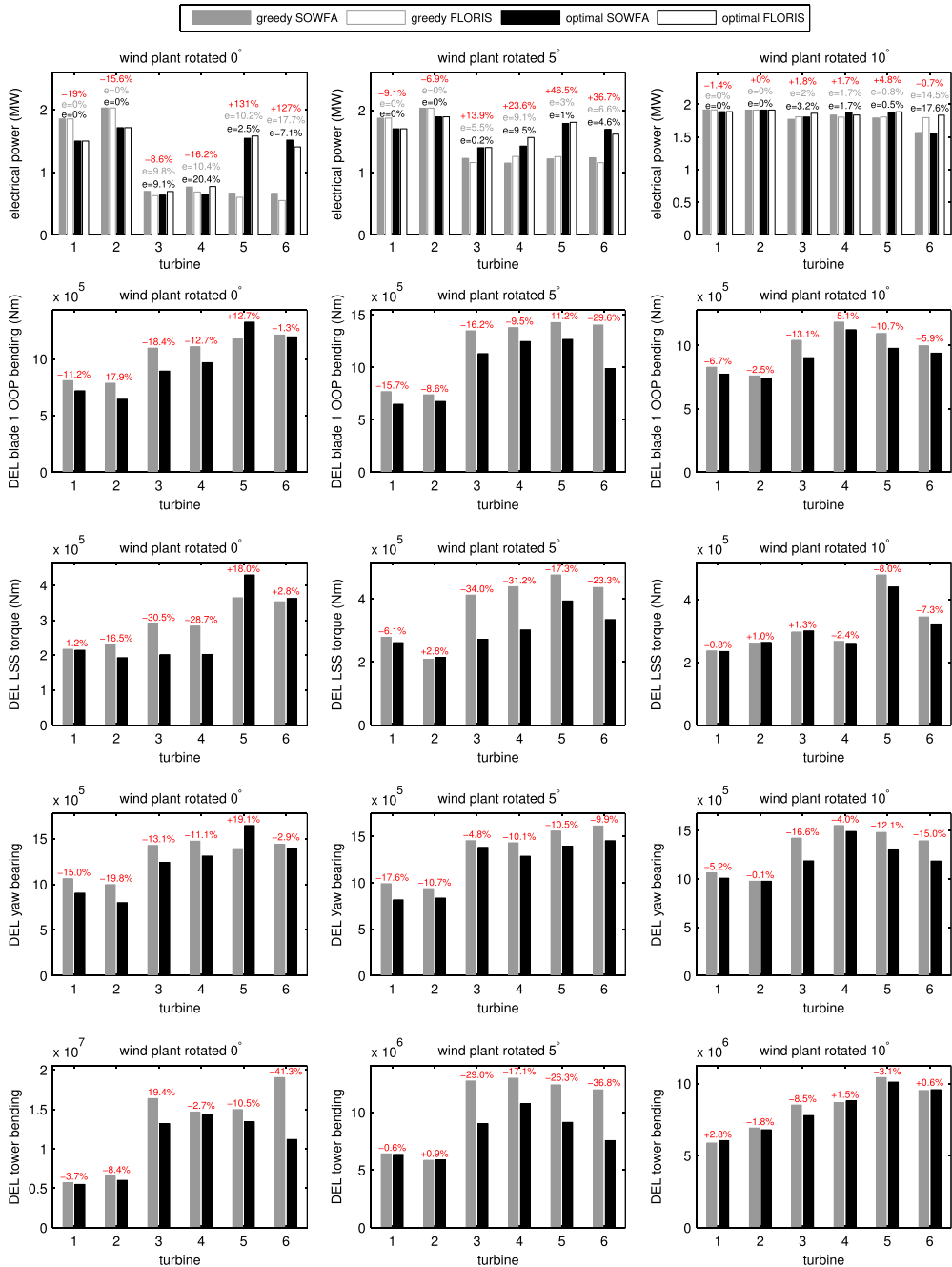


Figure 9. Time-averaged SOWFA simulation results (solid bars) for turbine electrical power production and structural loads for both turbine-level optimal (greedy) and plant-wide optimal yaw settings (optimal) and for three different wind plant configurations (see Figure 7 for these configurations). The data are averaged over a period of 50–500 s after plant-wide optimization control is switched on (and over the same period for the greedy case). Listed are increases of power and loads of the optimized case relative to the greedy case as calculated by SOWFA (in per cent, red). Also included are the FLORIS estimates of the power production levels (clear bars) and the associated errors e relative to the SOWFA-calculated values (in per cent, black and gray). Table II shows total wind plant electrical power production. Table III lists the yaw angles used in the optimal case.

Table III. Optimized turbine yaw angles (relative to the mean 30° wind direction) after 800 s of simulation for different wind plant configurations.

	Turbine 1	Turbine 2	Turbine 3	Turbine 4	Turbine 5	Turbine 6
Wind plant rotated 0°	25.85°	25.15°	39.80°	39.75°	0.45°	0.35°
Wind plant rotated 5°	19.00°	19.00°	23.80°	23.80°	0.05°	0°
Wind plant rotated 10°	6.25°	3.45°	4.75°	6.35°	-0.05°	0.05°

5.4. Overview of electrical power production and load results of simulations with different wind plant configurations

Table II shows the time-averaged results for the total wind plant electrical power production calculated with SOWFA and estimated with FLORIS for both greedy and plant-wide optimized settings for the 0°, 5° and 10° rotated configurations of the wind plant. Figure 9 shows the power production levels for each individual turbine. When comparing the FLORIS and SOWFA predictions of power production, we again see that there is not a perfect match, but the FLORIS predictions are accurate enough to enable a power production increase when using them for optimization of the yaw angles. In each of the cases with the plant-wide optimization controller, it can be seen that the loss of power through yawing on upstream turbines is compensated by a larger power gain in a downstream turbine. When comparing simulations with different configurations of the wind plant, we can see the effect of changes in the mean wind direction on the wake interaction in the wind plant—for a 10° rotation, the power production gain from the yaw optimization is much smaller. This is because in that case also with the greedy settings, there is little overlap of the wakes with the downstream turbines (see also the flow fields in Figure 7). Table III lists the optimal yaw angles as calculated by the GT optimization, which shows that in the case with the 10° rotated wind plant, the optimized yaw angles are much smaller.

Also included in Figure 9 are relevant structural loads on each turbine for each case, as estimated by the FAST dynamic model of each turbine. Note that the validation of load predictions from SOWFA is still an ongoing work. Loads are computed for blade out-of-plane bending moments, drivetrain low-speed shaft (LSS) torsion, yaw bearing moments and tower bending moments. For each of these load signals, we compute a damage equivalent load (DEL), which is a standard measure of fatigue damage.⁴⁵ The comparison shows that for most of the investigated loads, a reduction of DEL is observed when the yaw settings are optimized by the plant-wide controller, even though this was not the objective of the optimization. The observation that yaw misalignment on the upstream turbines can reduce the loads on these turbines themselves is consistent with the findings of Kragh and Hansen,²⁵ and load reductions on downstream turbines can be attributed to a reduction of wake overlap. There are increases in some DELs on some of the downstream turbines, which can be explained by an increase of imbalance through partial wake overlap. Fleming *et al.*²⁴ suggested that these loads can be mitigated using individual pitch control. Also, a drivetrain damper can mitigate the increase of loads on the LSS observed at turbine 5 for the 0° rotated wind plant case. We see substantial differences in the DELs when comparing the two 3-turbine rows in the wind plant, even though turbine spacing in each row is the same. This can be explained by the fact that the turbulence in the inflow is different for each of these rows and that the data are averaged over a relatively short period.

Finally, note that the expected beneficial effects of the proposed yaw optimization control on a large real wind plant are smaller than in this case study. In this case study, there is a relatively small spacing between the turbines in the flow direction, and a relatively slow wake recovery through mixing because of the low turbulence level in the inflow, and the neutral boundary layer conditions. These are conditions that make the wake losses relatively large in this wind plant, and consequently, we also see a large effect of mitigating these losses through control.

6. CONCLUSIONS

In this paper, we present a wind plant control strategy for optimizing the total electrical energy production of the wind plant by changing the yaw control set points of each turbine. The yaw control is used to change the direction and velocity of the wake forming behind each turbine in the wind plant. The optimization is based on predictions provided by the FLORIS model, a novel simplified parametric model for these wake effects in the wind plant.

In high-fidelity CFD simulation examples, we show that the control strategy could be applied successfully on a small wind plant. We found that the FLORIS model was able to predict the time-averaged turbine powers for both the greedy and plant-wide optimized settings with sufficient accuracy to yield a significant power production increase for different configurations of the wind plant. The CFD simulations also predict that a reduction of loads can be achieved through the yaw control. The CFD simulation examples provide a first proof of concept for the data-driven optimization scheme based on the FLORIS model.

Ongoing work is aimed at further developing the control scheme so that it can be applied on a real wind plant, under changing atmospheric conditions. When, for example, the turbulence intensity of the inflow changes, the wake properties are affected, and the model parameters should be updated online. The FLORIS model has a relatively simple formulation, with a small number of parameters that can be identified using power measurements of the different turbines in the wind plant. This enables the development of such a fully data-driven approach for adaptive wind plant optimization control.

In further ongoing work by the authors of this paper and others, the FLORIS model is being extended with a more accurate description of the wake effects, in order to give better predictions of the wind plant performance. This work includes the extensions proposed by Annoni *et al.*,⁴⁶ consisting of a better description of wake decay through turbulent mixing in overlapping wakes and a better prediction of the effects of changing axial induction using blade pitch and generator torque. In addition, in the work of Gebraad and van Wingerden,⁴⁷ the FLORIS model is extended with dynamic effects by including the delays associated with the wake effects propagating through the wind field.

Certainly, when considering varying atmospheric conditions, the FLORIS model needs to be further validated. Gathering validation data from relevant and realistic scenarios with changing wind conditions from high-fidelity models like SOWFA, or with a real wind plant, is a substantial task given the computational costs of high-fidelity models and the uncontrollable nature of the conditions in real wind plant. With proper validation of the model under varying wind conditions, a description of the uncertainty of the FLORIS model should also be formulated. This uncertainty description would enable a robust yaw control strategy to be developed, possibly with some conservatism in the amount of yaw offset used.

ACKNOWLEDGEMENTS

This work is supported by the Far Large Offshore Wind project no. 201101 ‘Offshore wind power plant control for minimal loading’ and by the NWO Veni Grant no. 11930 ‘Reconfigurable floating wind plant’. The contribution of the National Renewable Energy Laboratory (NREL) to this work were supported by the US Department of Energy under contract no. DE-AC36-08GO28308 with NREL.

REFERENCES

- Vermeer LJ, Sørensen JN, Crespo A. Wind turbine wake aerodynamics. *Progress in Aerospace Sciences* 2003; **39**(6-7): 467–510.
- Crespo A, Hernández J, Frandsen S. Survey of modelling methods for wind turbine wakes and wind farms. *Wind Energy* 1999; **2**(1): 1–24.
- Sanderse B, *Aerodynamics of wind turbine wakes*, Technical Report ECN-E-09-016, Energy Centre of the Netherlands, 2009.
- Ainslie JF. Calculating the flowfield in the wake of wind turbines. *Journal of Wind Engineering and Industrial Aerodynamics* 1988; **27**(1-3): 213–224.
- Dahlberg J, Medici D. Potential improvement of wind turbine array efficiency by active wake control. *Proceedings of European Wind Energy Conference*, Madrid, Spain, 2003; 65–84.
- Wagenaar JW, Machielse L, Schepers J. Controlling wind in ECN’s scaled wind farm. *Proceedings of the EWEA Annual Meeting*, Copenhagen, Denmark, 2012.
- Jiménez Á, Crespo A, Migoya E. Application of a LES technique to characterize the wake deflection of a wind turbine in yaw. *Wind Energy* 2010; **13**(6): 559–572.
- Johnson KE, Thomas N. Wind farm control: addressing the aerodynamic interaction among wind turbines. *Proceedings of the American Control Conference*, St. Louis, MO, USA, 2009; 2104–2109.
- Barthelmie R, Frandsen S, Hansen K, Schepers J, Rados K, Schlez W, Neubert A, Jensen L, Neckelmann S. Modelling the impact of wakes on power output at Nysted and Horns Rev. *Proceedings of the European Wind Energy Conference*, Marseille, France, 2009.
- Steinbuch M, de Boer WW, Bosgra O, Peters S, Ploeg J. Optimal control of wind power plants. *Journal of Wind Engineering and Industrial Aerodynamics* 1988; **27**: 237–246.
- Bitar E, Seiler P. Coordinated control of a wind turbine array for power maximization. *Proceedings of the American Control Conference*, Washington, DC, USA, 2013; 2898–2904.
- Jensen NO, *A note on wind generator interaction*, Technical Report Risø-M-2411, Risø National Laboratory, 1984.
- Katić I, Højstrup J, Jensen NO. A simple model for cluster efficiency. *Proceedings of the European Wind Energy Association Conference and Exhibition*, Rome, Italy, 1986; 407–410.

14. Gonzalez JS, Payan MB, Santos JR. Optimal control of wind turbines for minimizing overall wake effect losses in offshore wind farms. *Proceedings of EUROCON*, Zagreb, Croatia, 2013; 1129–1134.
15. Frandsen S, Barthelmie R, Pryor S, Rathmann O, Larsen S, Højstrup J, Thøgersen M. Analytical modelling of wind speed deficit in large offshore wind farms. *Wind Energy* 2006; **9**(1-2): 39–53.
16. Schepers JG, van der Pijl SP. Improved modelling of wake aerodynamics and assessment of new farm control strategies. *Journal of Physics: Conference Series* 2007; **75**(1): 012039.
17. Marden JR, Ruben SD, Pao LY. A model-free approach to wind farm control using game theoretic methods. *IEEE Transactions on Control Systems Technology* 2013; **21**(4): 1207–1214.
18. Gebraad PMO, van Wingerden JW. Maximum power-point tracking control for wind farms. *Wind Energy* 2014.
19. Heer F, Esfahani PM, Kamarpour M, Lygeros J. Model based power optimisation of wind farms. *Proceedings of the European Control Conference*, Strasbourg, France, 2014; 1145–1150.
20. Soleimanzadeh M, Wisniewski R, Kanev S. An optimization framework for load and power distribution in wind farms. *Journal of Wind Engineering and Industrial Aerodynamics* 2012; **107-108**: 256–262.
21. Soleimanzadeh M, Wisniewski R. Controller design for a wind farm, considering both power and load aspects. *Mechatronics* 2011; **21**(4): 720–727.
22. Soleimanzadeh M, Wisniewski R, Johnson K. A distributed optimization framework for wind farms. *Journal of Wind Engineering and Industrial Aerodynamics* 2013; **123**: 88–98.
23. Fleming PA, Gebraad PMO, Lee S, van Wingerden JW, Johnson K, Churchfield M, Michalakes J, Spalart P, Moriarty P. Evaluating techniques for redirecting turbine wakes using SOWFA. *Renewable Energy* 2014; **70**: 211–218.
24. Fleming P, Gebraad PMO, Lee S, van Wingerden JW, Johnson K, Churchfield M, Michalakes J, Spalart P, Moriarty P. Simulation comparison of wake mitigation control strategies for a two-turbine case. *Wind Energy* 2014.
25. Kragh KA, Hansen MH. Load alleviation of wind turbines by yaw misalignment. *Wind Energy* 2013; **17**(7): 971–982.
26. González-Longatt F, Wall P, Terzija V. Wake effect in wind farm performance: steady-state and dynamic behavior. *Renewable Energy* 2012; **39**(1): 329–338.
27. Choi J, Shan M. Advancement of Jensen (Park) wake model. *Proceedings of the EWEA Annual Meeting*, Vienna, Austria, 2013.
28. Gebraad PMO, Teeuwisse FW, van Wingerden JW, Fleming PA, Ruben SD, Marden JR, Pao LY. A data-driven model for wind plant power optimization by yaw control. *Proceedings of the American Control Conference*, Portland, OR, USA, 2014.
29. Yang X, Sotiropoulos F. On the predictive capabilities of LES actuator disk model in simulating turbulence past wind turbines and plants. *Proceedings of the American Control Conference*, Washington, D.C., USA, 2013; 2878–2883.
30. Larsen GC, Madsen HA, Bingöl F, Mann J, Ott S, Sørensen JN, Okulov V, Troldborg N, Nielsen M, Thomsen K, Larsen TJ, Mikkelsen R, *Dynamic wake meandering modeling*, Technical Report Risø-R-1607(EN), Risø National Laboratory, 2007.
31. Churchfield MJ, Lee S, Michalakes J, Moriarty PJ. A numerical study of the effects of atmospheric and wake turbulence on wind turbine dynamics. *Journal of Turbulence* 2012; **13**(14): 1–32.
32. Schepers JG, van der Pijl SP. Improved modelling of wake aerodynamics and assessment of new farm control strategies. *Journal of Wind Engineering and Industrial Aerodynamics* 2007; **75**(012039).
33. Park J, Kwon S, Law KH. Wind farm power maximization based on a cooperative static game approach. *Proceedings of the SPIE Active and Passive Smart Structures and Integrated Systems Conference*, San Diego, CA, USA, 2013.
34. Jonkman J. NWTC design codes (FAST). Available: <http://wind.nrel.gov/designcodes/simulators/fast> (Accessed July 2013).
35. Fleming P, Gebraad P, van Wingerden JW, Lee S, Churchfield M, Scholbrock A, Michalakes J, Johnson K, Moriarty P. The SOWFA super-controller: a high-fidelity tool for evaluating wind plant control approaches. *Proceedings of the EWEA Annual Meeting*, Vienna, Austria, 2013.
36. Fleming P, Gebraad P, Churchfield M, Lee S, Johnson K, Michalakes J, van Wingerden JW, Moriarty P, *SOWFA + super controller user's manual*, Technical Report NREL/TP-5000-59197, National Renewable Energy Laboratory, 2013.
37. Churchfield M, Lee S, Moriarty P, Martinez L, Leonardi S, Vijayakumar G, Brasseur J. A large-eddy simulation of wind-plant aerodynamics. *Proceedings of the AIAA Aerospace Sciences Meeting*, Nashville, Tennessee, USA, 2012.
38. Jonkman J, Butterfield S, Musial W, Scott G, *Definition of a 5-MW reference wind turbine for offshore system development*, Technical Report NREL/TP-500-38060, National Renewable Energy Laboratory, 2009.

39. Burton T, Sharpe D, Jenkins N, Bossanyi E. Wind energy handbook. In *Wind Energy Handbook*. John Wiley and Sons, Ltd: Chichester, UK, 2002; 471–509.
40. Bianchi FD, Battista HD, Mantz RJ. *Wind Turbine Control Systems; Principles, Modelling and Gain Scheduling Design*. Springer-Verlag: London, UK, 2007.
41. Medici D. Experimental studies of wind turbine wakes: power optimisation and meandering, *PhD Thesis*, KTH Royal Institute of Technology, 2005.
42. Annoni J, Seiler P, Johnson K, Fleming P, Gebraad P. Evaluating wake models for wind farm control. *Proceedings of the American Control Conference*, Portland, OR, USA, 2014.
43. Hau E. Control systems and operational sequence. In *Wind Turbines—Fundamentals, Technologies, Application, Economics*. Springer: Berlin Heidelberg, 2013; 429–465.
44. Kragh KA, Fleming PA, Scholbrock AK. Increased power capture by rotor speed-dependent yaw control of wind turbines. *Journal of Solar Energy Engineering* 2013; **135**(3).
45. Buhl Jr. M, *MCrunch theory manual for version 1.00*, Technical Report NREL/TP-500-43139, National Renewable Energy Laboratory, 2008.
46. Annoni J, Gebraad PMO, Scholbrock AK, Fleming P, van Wingerden JW. Analysis of axial-induction-based wind plant control using low-order and high-order wind plant models, 2014. To appear.
47. Gebraad PMO, van Wingerden JW. A control-oriented dynamic model for wakes in wind plants. *Proceedings of the Science of Making Torque from Wind*, Lyngby, Denmark, 2014.